Mechanism of olivine and glass alteration under experimental H2O-CO2 based supercritical gas: Application to modern and ancient Venus

Jérôme Esvan, Gilles Berger, Sébastien Fabre, Eric Bêche, Yannick Thébault, Alain Pages, Cédric Charvillat

MECHANISM OF OLIVINE AND GLASS ALTERATION UNDER EXPERIMENTAL H_2O-CO_2 BASED SUPERCRITICAL GAS: APPLICATION TO MODERN AND ANCIENT VENUS.

Jérôme Esvan[1], Gilles Berger[2*], Sébastien Fabre[3], Eric Bêche[4], Yannick Thébault[1], Alain Pages[2] and Cédric Charvillat[1]

[1] CIRIMAT, CNRS-UPS-INPT, ENSIACET, 4 allée Emile Monso, 31030 Toulouse, France

[2] IRAP, CNRS, Observatoire Midi-Pyrénées, 14 av. Edouard Belin, 31400 Toulouse, France

[3] IRAP, Université Paul Sabatier, Observatoire Midi-Pyrénées, 14 av. Edouard Belin, 31400 Toulouse, France

[4] PROMES, PCM-ASI-CNRS, 7 rue du Four Solaire, 66120 Font-Romeu, France

* corresponding author: gilles.berger@irap.omp.eu

keywords: experimental; supercritical alteration; olivine; glass; surface spectroscopy; Venus

Abstract:

Extreme conditions encountered in some geological contexts (deep serpentinization, interaction of Venus atmosphere with its basaltic surface, volcanic degassing) activate mechanisms and rates of silicate alteration that are poorly understood. In the present study, we investigate the mechanisms of mineral reactions in a natural geological system at high temperature, under conditions where the low solvation of cations by fluids likely promotes surface reactions such as surface diffusion and/or local recrystallization. We focus on vitreous glasses and olivine, reputed to be the most alterable phases in volcanic rocks, by reacting samples for one week in a Ni-based alloy experimental vessel. For the framework of our experimental study, we chose to apply the deep atmosphere conditions on Venus: 470°C and 90 bar of reconstituted Venus-like gas. We also tested the effect of water (Early Venus or wet volcanic degassing) by adding water vapor at up to 320 bar total pressure. The mineral reactions affecting the samples were identified by a set of spectroscopic surface analyses of the altered samples: Scanning Electron Microscopy, Energy Dispersive X-ray Spectroscopy, X-Ray Diffraction in grazing incidence mode, X-ray Photo electron Spectroscopy and Raman spectroscopy.

Samples of obsidian and tholeiitic glasses are found to be sensitive to a threshold water pressure, depending on glass composition, below which the reaction is limited to some elemental mobility in the glass (alkali enrichment, calcium loss) leading to a possibly more stable surface layer of tens to hundreds of microns. Above this threshold water pressure (ca. 50 bar H_2O for the obsidian but >250 bar H_2O for the tholeiitic glass), water promotes the depolymerization of the glass and the crystallization of stable minerals. This crystalline rim is less protective that the chemically modified layer.

Olivine samples react differently depending on whether the olivine is isolated or included in a basaltic rock. In the latter case only, iron coatings are formed, which are identified as hematite, suggesting that this phase is not fed by olivine itself but rather by surface diffusion from neighboring Fe-rich phases. This supports the conclusions from experimental studies and orbital observations on the short-term visibility of unaltered olivine in Venus lava flows: such a coating is enhanced when Fe-bearing minerals are in the proximity of olivine. Under high water vapor pressure, Fe-bearing talc (and not serpentine) forms by a likely topotactic reaction that also incorporates silica from the gas. This talc layer may form a protective layer, implying that serpentinization of ultramafic rocks at high temperature may not be as prevalent as one might think in a gas-dominated system like the Early Venus surface.

1 - Introduction:

The mechanisms and rates of rock alteration by liquid water in weathering and hydrothermal processes have been investigated for decades. By contrast, the alteration of silicate phases in contact with gas or supercritical fluids is less well documented. In the petroleum field, it is well accepted that diagenesis is negligible in gas reservoirs, suggesting a lower reactivity of the mineral matrix with the gas, at least at temperature below 200°C. In the literature on CO_2 sequestration, more extensive experimental studies are available showing the importance of gas humidity. A critical factor in many mineral carbonation reactions in supercritical CO2 is the formation of adsorbed water films on the mineral surfaces. For example, Daval *et al.* (2005) observed the carbonation of wollastonite in experiments conducted in supercritical CO_2 at 90 °C and 250 bar equilibrated with water pressure. Using the mutual solubility of CO_2 and H_2O reported in Spycher et al. (2003) for similar temperature and pressure conditions, the molar fraction of H_2O in the supercritical CO_2 phase ($scCO_2$) is of the order of 1.4%. This available water likely promotes the propagation of carbonation of wollastonite. In another study, Regnault *et al*., (2009) reacted pure $scCO_2$ with portlandite [$Ca(OH)_2$] up to 200°C and reported a significant carbonation of the mineral samples. The above authors (*op.cit*.) attributed this reaction to a direct interaction of molecular H_2O (from portlandite) and CO_2 with the mineral surface. The recent review of Miller *et al.* (2019) summarized 15 studies on the carbonation of olivine in H_2O-saturated supercritical CO_2, showing that olivine carbonation is optimized at 185-200 °C. The mechanism by which water promotes carbonation is described in detail by Thompson *et al.* (2013): a sorbed layer first allows CO_2 hydration, with the formation of carbonic acid (which dissociates into protons and bicarbonate ions), and then dissolution of the silicate surface by the local acidity.

On the other hand, in strictly dry CO_2 fluids, the very low dielectric constant of non-polar fluids makes the breakdown of the silicate structure improbable whatever the Gibbs free energy of reaction. However, at elevated temperatures, other reactions than ion solvation may operate in a dry gas. Staub and Burns (1991) reported oxidation of ferromagnesian silicates at 800°C under 1 atmosphere of dry CO_2. More generally, the reactions of volcanic gas (CO_2, SO_2) with ash during a volcanic eruption were recently reviewed by King *et al.* (2018), Delmelle *et al.* (2018), Renggli and King (2018) and Palm *et al.* (2018). These reviews illustrate the importance of gas-rock reactions at very high temperature.

At intermediate temperatures, Venus is an interesting case: its deep atmosphere is hot (470°C), dry (few tens ppm H_2O) and composed of a low-density CO_2-based gas. Understanding the potential interactions between the atmosphere and the basaltic surface is a

challenge for better interpreting the remote spatial observations of past or incoming missions. Zolotov (2018) reviewed the alteration pathways expected on the surface of Venus and discussed possible mineral parageneses from thermodynamic considerations (magnetite/hematite competition, olivine and pyroxene stability, sulfatization and carbonatization, etc.).This latter author concludes that, under both present and past conditions on Venus, the rates, mechanisms and alteration products remain so far unknown. A recent study by Berger *et al.* (2019) describes the reactions of silicate materials exposed to a CO_2-based gas at temperatures approaching 500°C. Their experimental study demonstrates that the key factor in dry gas is oxidation: namely, oxidation of iron below the surface of glasses and oxidation of SO_2 at the mineral-gas interface. This results in the precipitation of oxidized products onto the reacted surfaces, i.e. sulfate for the glass and iron oxide for the olivine.

In the present study, we address the mechanisms of glass and olivine alteration in H_2O-CO_2 based supercritical fluids. We focus on conditions relevant to modern-day and ancient Venus (dry and wetter climates, respectively) as well as wet volcanic degassing. We focus mainly on low-density supercritical fluids at 470°C containing traces of CO and SO_2, in continuation with the studies of Berger *et al.* (2019). These conditions correspond more specifically to modern-day conditions on the Venus plains. However, we also performed a run at 300°C to simulate conditions on the Venus Highlands. Beside Venus, our study addresses the more general question of serpentinization of ultramafic rocks. We pay particular attention to the passivation mechanism that limits the reaction in a natural geological system at high temperatures, conditions at which the low solvation of cations likely promotes other surface reactions such as surface diffusion and/or local recrystallization.

2 – Procedure

2.1 – Experimental

Rock samples were allowed to react under supercritical conditions in a 300 mL bolted reactor from Autoclave France®. The reactor is made of Hastelloy C-276, a Ni based alloy which is relatively inert with respect to acid gas (CO_2, SO_2 or H_2S) and which contributes to buffering the redox conditions close to modern Venus surface conditions. For these reasons, this set-up was used in previous studies to measure the solubility of CO_2-H_2S gas mixtures in the context of sour gas sequestration in depleted petroleum reservoirs (Savary *et al.*, 2012) and more recently for modelling the deep atmosphere of Venus (Berger *et al.*, 2019). More details of the experimental procedure can be found in these two papers cited above. In the present study, the reactor was configured and used under conditions typical of the surface of the modern Venus

plains, i.e. 475°C and 90 bar, with a reconstituted CO_2-based Venus gas containing 4.5% N_2, hundreds of ppm of SO_2, H_2S and tens of ppm CO. Before heating, and after flushing with Ar to eliminate oxygen, the reactor was filled with a CO_2-9% N_2-390ppm SO_2 mixture up to 25 bar and then completed to 50 bar by pure CO_2. The final pressure was in the range of 85-95 bar after heating.

Water was injected into the reconstituted Venus gas to model ancient conditions on Venus, as well as deep-earth aqueous supercritical fluids and wet volcanic degassing. The effect of water was tested by applying an additional water pressure, up to 250 bar (350 bar total pressure) for the extreme case. This higher water pressure, although outside the range Venus conditions, allows exploration of silicate hydrolysis as a function of H_2O fugacity. H_2O fugacity was calculated from the mass of injected water, along withtemperature and pressure monitoring data using the EOS computer package (Bakker, 2009). The typical duration was one week. At the end of the run, the pressure was released before cooling of the reactor in order to avoid any reaction during the cooling. During this operation, the concentration of CO, H_2S and SO_2 in the gas was measured by a GasAlertMicro5 gas controller available from BW-Technologies®. The in-situ O_2 fugacity was calculated from the CO/CO_2 ratio as given in Berger *et al.* (2019). In one case, we performed a direct measurement of fO_2 with a SENTAC Jok'Air oxygen analyzer and thus validated the CO/CO_2 method. The in-situ O_2 fugacity was likely controlled by the Ni-NiO couple at the surface of the reactor (Ni-based alloy), below the hematite-magnetite buffer, and corresponds roughly to the assumed conditions prevailing in the Venus deep atmosphere (Fegley *et al.*, 1997).

Two experiments were conducted outside the conditions described above. One run was conducted at 300°C, 15 bar H_2O (vapor phase) to test to what extent our results are relevant for Venus highlands conditions. Another run was conducted at 470°C, but in Ar-10%H_2, to check the dependence of the surface reaction to redox conditions.

The experimental conditions are summarized in Table1.

Run	T (°C) ±3°C	duration (day)	$X(H_2O)$	density initial	$P_{initial-final}$ (bar)	$H_2O_{initial}$ (MPa)	CO ppmv	H_2S	SO_2 ppmv	log fO_2
V24	474	7	0	0.070	98	0	/	/	37	/
V25	473	7	0	0.065	102-94	0	28	15	120	-21.0
V26	474	7	0.73	0.130	246-248	14.0	17	38	28	-21.3
V27	474	7	0.94	0.174	325-315	21.4	155	740	8	-22.8
V28	299	7	1	0.006	17-15	1.55	/	/	/	/
V29	473	7	0.85	0.173	354-333	20.8	>0.4%	172	4	-20.5 *(by Jok'Air)*

(Ar-10%H_2 as background gas)

***Table 1**: Experimental conditions for reaction of basalt glass and olivine under Venus conditions. X(H_2O) is the molar ratio of water in the gas and d the density at the working temperature.*

2.2 - Samples:

We focus here on the two most reactive materials in the upper crust, Fe-forsterite and basalt glass, by exposing them to alteration as cm-sized crystals or slabs suspended in a Pt crucible. The comparison of the alteration thickness after one week of reaction between different materials is informative of the alteration kinetics.

The choice of the glass compositions, from tholeiitic to alkaline, allows us to cover a wider diversity of basaltic rocks than those resulting from the late-stage resurfacing of Venus. This is because the ancient surface composition of Venus is not constrained by current exploration data.

The tholeiitic glass was produced by melting a natural and unaltered tholeiitic basalt under anoxic conditions (Pic d'Ysson, Massif Central, France). The alkaline glass was the same material used in Berger *et al.*'s (2019) study. For olivine, we tested two natural Fe-forsterites: cm-sized samples of San Carlos crystals and olivine phenocrysts in a picritic basalt. The picritic basalt hosting the olivine phenocrysts was collected in a recent lava flow of the Piton de la Fournaise on Réunion Island. The composition of the experimented material is reported in Table 2. For the run conducted at 300°C, we also used a natural obsidian sample, previously studied in Berger *et al.* (2019). The mineral reactions affecting the surface samples were identified by microanalyses of the altered samples: Scanning Electron Microscopy (SEM), Energy Dispersive X-ray Spectroscopy (SEM), X-Ray Diffraction (XRD), X-ray Photo electron Spectroscopy (XPS) and Raman spectroscopy, with each analytical method probing a specific thickness of the sample: a few nm for XPS, 1-2 µm for Raman, 3 µm for EDS and XPS as well as for XRD. The progression rate of the mineral/chemical alteration inside the material was measured on polished sections.

Sample	SiO_2	Al_2O_3	FeO(t)	CaO	MgO	Na_2O	K_2O	TiO_2	MnO
San Carlos olivine	48.7	0	9.2	0	49.2	-	-	-	-
olivine in picritic basalt	37.8	0	17.8	0.4	43.0	-	-	-	-
tholeiitic glass	40.2	11.1	13.1	10.4	13.1	3.5	1.5	2.5	0.3
natural obsidian (*)	*73.1*	*13.4*	*2.3*	*1.03*	*0.19*	*4.19*	*5.25*	*0.11*	*0.08*

***Table 2**. Chemical composition of the staring samples. (*) described in Berger et al. (2019)*

2.3 - Analytical methods

Scanning Electron Microscopy (SEM) observations were performed with VFEI Quanta450 microscope equipped with a Brucker® Quantax EDS system, in both secondary electron imaging mode (SEI) and/or backscattering electron mode (BSE) on carbon-coated samples or polished sections. The analytical conditions for point chemical analyses were 15 kV, 10^6 counts and a working distance of 10 mm. Quantitative data were obtained using the Phi(RhoZ) matrix correction method. A maximum error of +-2% is reasonable owing to the use of reference materials in a true standards library and a minimum of 200k counts per analysis point. A closely similar carbon coating covers both the analyzed specimen and the standards.

X-Ray Diffraction (XRD) analyses were performed on a *Bruker® D8* ADVANCE XRD diffractometer ($CuK\alpha^{1+2}$ radiation) over the 2-60°2Θ angular range with 0.02°2Θ steps and 2 s per step. The apparatus is configured for grazing incidence X-ray diffraction (GIXRD) with a solid-state detector used in 0 dimension and a Göbel mirror. The different incidences of X-rays on the sample were fixed at 0.5, 1, 2 and 5°. *Bruker* AXS software (AbsorbDX) predicts a penetration depth of ≈ 0.6 µm with a grazing angle of 0.5°and 3.8 µm with a grazing angle of 5°.

X-ray Photo electron Spectroscopy (XPS) analyses were performed on a *ThermoScientific®* spectrometer (Kalpha) using a monochromatized Al Kα source (1486.6 eV). The Pass energy was fixed at 40 eV with a step size of 0.1 eV for core levels and 160 eV (step size of 1 eV) for surveys. XPS Spectra were recorded in direct energy form N(Ec). The analyzed surface area is 400 µm in diameter and less than 10 nm in depth. A Flood Gun was turned on to neutralize surface charges. The photoelectron spectra were calibrated with respect to the C1s peak at 284.6 eV (+/- 0.1eV) energy. XPS data were fitted by using Thermo Scientific Avantage Software and the Shirley method was used for background subtraction of all the peaks.

Raman experiments were performed using a HORIBA LabRAM HR evolution Raman spectrometer equipped with an optical microscope (Olympus BX 41, x10 WD, x50 (long working distance (LWD)), x100 WD objective lens), a Charge Coupled Device detector (1024 x 256 pixels, 26□m by pixel) and two laser beams (HeNe laser wavelength = 633 nm, laser power=17 mW and laser diode wavelength = 532 nm, laser power=39 mW). The Raman shift was calibrated using a standard sample of silicon.

The measurements were performed at room temperature (293 K). Raman spectra were recorded in the wavenumber range (spectral region) of 150 to 1500 cm-1. The excitation source was a 532 nm laser beam and its power was reduced to about 19 mW (filter=50%) to avoid laser induced effects (surface heating by the source). No effects were observed. The Raman spectra were collected at the focal point of the objective lens (x50 (NA=0.75) or x100 (NA=0.9)) with a spectral resolution close to 1 cm^{-1}/pixel. A 1800 gr/mm grating and a confocal pinhole value of 50 or 100 µm were selected. The acquisition time and the number of acquisitions per analysis point were fixed at 20 s and 5, respectively. The Raman spectra were collected using Horiba software (LabSpec 6.0).

3 – Results

3.1 - Behavior of basalt glass at 475°C:

In a dry Venus-like atmosphere, basalt glass shows growth of Na-Ca-sulfate crystals as already reported and extensively discussed in Berger *et al.* (2019). Therefore, we do not go into further detail about this observation. In wet gas, basalt glass presents, in addition, a chemically modified layer below the surface as shown by SEM in Figure 1 (70 µm thick for the run using the higher vapor pressure). Although the sulfate crust exists, resulting from the oxidation of gaseous sulfur species, it is barely visible at the scale of the figure, and could not be analyzed in cross-section. EDS analysis of the modified layer in cross-section shows complex chemical profiles, in particular for calcium and the alkalis. These chemical variations are qualitatively consistent with XPS observations at a nanometer scale reported in Berger *et al.* (2019) for the same glass altered under dry conditions. However, the presence of water in the gas enhances the magnitude of the cation mobility: tens to hundreds of µm in wet gas as against only hundreds of nm under dry gas, as reported by Berger *et al.* (2019).

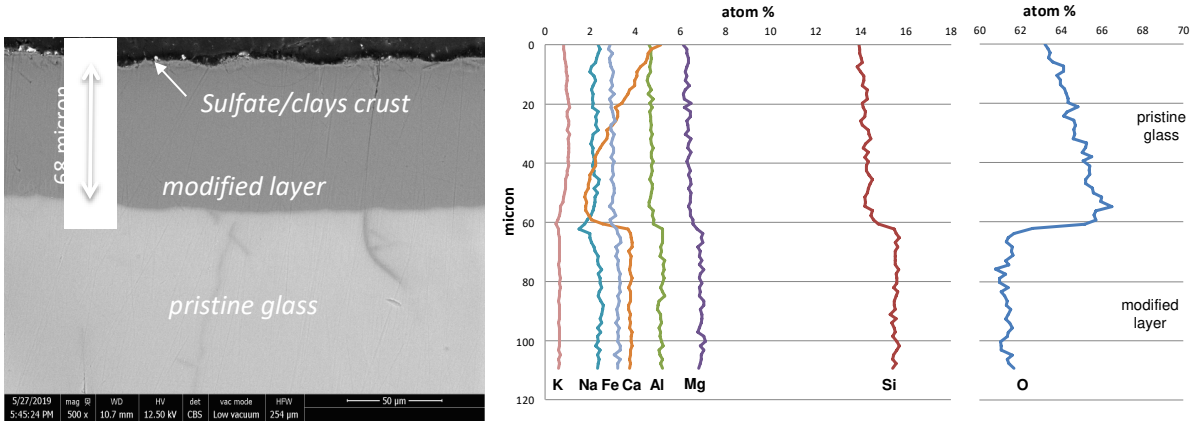

Figure 1: SEM observation in backscattering mode of the modified layer in a reacted tholeiitic glass sample altered under high vapor pressure (V27, polished section). Linescans of EDS point analyses in the modified layer are reported on the right.

Using the thickness of the leached layer obtained after a constant reaction run-time of one week as a proxy of alteration kinetics, our experiments at various water pressures indicate that the thickness of this layer increases regularly, but not linearly, with water fugacity in the gas, demonstrating that H_2O plays a role in cation diffusion (Figure 2).

3.2 – Comparison with obsidian:

By contrast with the results obtained by Berger *et al.* (2019) with an obsidian glass in a wet gas, we do not observe any deep recrystallization of the tholeiitic glass into stable mineral phases (plagioclase and mafic minerals in the case of obsidian), even under hundreds of bars of water pressure. A modest crystalized rim was observed by Berger *et al.* (2019) in the case of tholeiitic glass altered at 475°C but at very high water pressure (500 bar), with the formation of stable secondary phases consisting of phyllosilicates. By contrast with obsidian, the complete recrystallization of the glass requires much higher water pressure. We can also assume that chemical modifications are likely to occur in obsidian prior to complete recrystallization of the glass, but they are overprinted by the rapid crystallization process. The dominant run product is represented here either by an altered layer or a recrystallized rim; Figure 2 shows the progression of the altered surface layer after one week for the two glasses. For the tholeiite glass, as in the case of obsidian, we observe a threshold fH_2O below which no reaction is detected, but the value is approximately three times higher than with obsidian. In addition, we also note that rim thickness is dependent on fH_2O.

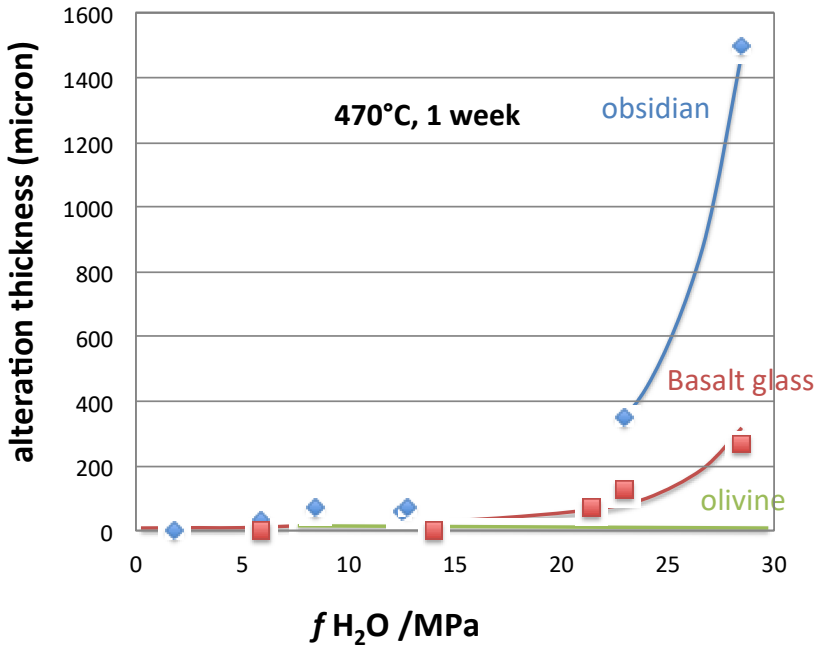

Figure 2: Dependence of tholeiitic glass alteration thickness on water fugacity, compared with the recrystallized rim thickness of obsidian glass reported in Berger et al. (2019). The vertical dashed lines indicate the threshold values for the onset of alteration.

Obsidian and basalt glass are altered according to two different mechanisms: fast depolymerization and recrystallization for the former, diffusion of modifier cations (Ca, alkalis) without depolymerization for the latter. The reason for this difference between the dominant processes is unclear and may be related to crystallographic features or a passivation effect due to iron in the case of the basaltic glass, its Fe content being significantly higher than in obsidian. To test this last hypothesis, a run was conducted in Ar-10%H_2 gas (V29, Table 2). But the chemical buffer of the reactor (Hastelloy, graphite gasket) did not lead to a significant lowering of oxygen fugacity and the alteration product was similar to the run in Venus gas, thus not providing a definitive conclusion.

3.3 – Effect of temperature on glass alteration:

The experiment carried out at 300°C with tholeiitic glass in water vapor did not give rise to any alteration features (nor on San Carlos olivine). The obsidian glass, on the other hand, displays a deep chemical zoning below the surface as shown in Figure 3, but without recrystallization as observed at high temperature and water pressure. This modified layer is similar to that observed in the tholeiitic glass at 475°C, supporting the hypothesis that both

processes - elemental diffusion and recrystallization - may affect the glass whatever its composition, depending on temperature and $f\,H_2O$.

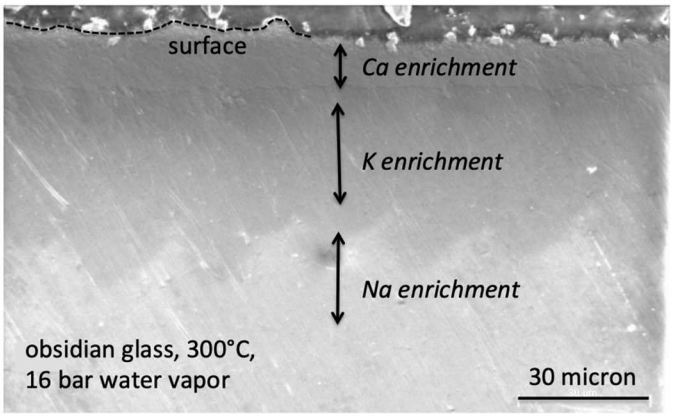

Figure 3: SEM observation in backscattering mode of the leached layer in an obsidian glass sample reacted in water vapor at 300°C (V28, polished section). The accumulation of elements is visible by the color contrast (elemental compositions measured by EDS)

3.4 - Behavior of San Carlos olivine:

When performing runs with single San Carlos samples, we failed to reproduce the iron oxide coatings reported by Berger *et al.* (2019), neither in dry nor in wet gas. We nevertheless observed a lamellar aspect under SEM (Figure 4) at the surface of samples altered under high water vapor pressure (V26 and V27).

Analysis by XRD in grazing incidence mode allowed us to determine the in-depth distribution of various crystalline phases by varying the X-ray incidence angle and thus controlling the penetration depth. We obtained the diffraction pattern of a 2:1 phyllosilicate, with reflections at 9.42 Å, 4.72 Å and 3.134 Å, corresponding to the (00l) planes. Given the context, we consider that talc ($Mg_3Si_4O_{10}(OH)_2$) is likely to be present. However, the peak at 30 Å, which is not typical of talc, may reflect an unusual superstructure. The absence of other reflections suggests a particular orientation of the flakes.

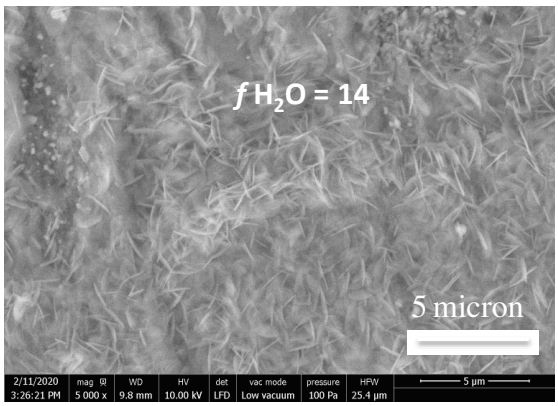

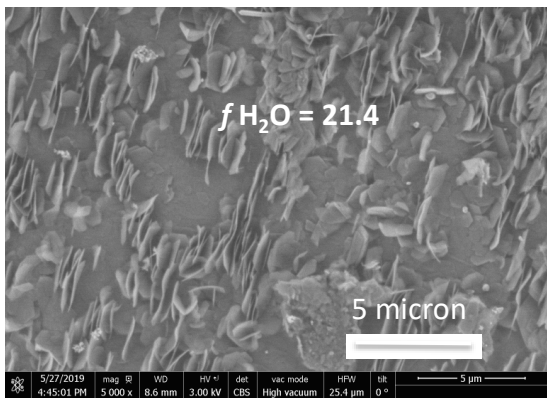

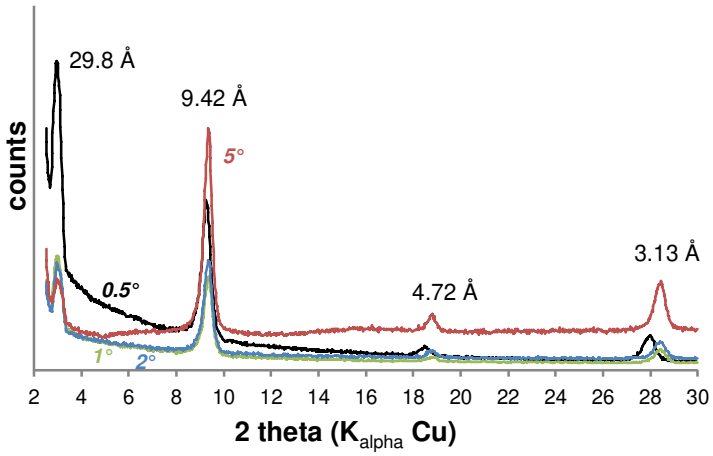

Figure 4: SEM images of single San Carlos crystals reacted one week at 475°C under 247 bar (upper left) and 320 bar (upper right) H_2O-CO_2 pressure, with XRD pattern of the surface in grazing incidence.

The presence of talc is supported by Raman spectroscopy (Fig. 5). The main Raman peaks observed in the wavenumber (ν) range of 750 cm^{-1} to 1000 cm^{-1} are similar to those from an unaltered olivine sample. The main Raman peaks (P1 and P2), located in the 750-1100 cm^{-1} window at 822.9 cm^{-1} and 855.1 cm^{-1}, result from mixed ($\nu_1 + \nu_3$) contributions (Parques-Ledent and Tarte, 1973, Piriou and McMillan, 1983). For these Raman spectra (crystallographic orientation near [010] axis, $I_{P1} >> I_{P2}$), the contribution of the ν_1 vibration mode (Ag symmetry mode, symmetric SiO_4 stretching) to the P1 peak is higher than the contribution of the ν_3 vibration modes (Ag symmetry mode, asymmetric SiO_4 stretching). Several authors (Kuebler *et al.*, 2006, Ishibashi *et al.*, 2008, Breitenfeld *et al.*, 2018) have related olivine composition using Raman spectroscopy to the P1 and P2 peak shift and identified variations in olivine Raman spectra based on the composition of individual olivine grains. The amount of forsterite (Fo) is positively correlated with peak shift (Kuebler *et al.*, 2006). According to the results of these latter authors, the estimated chemical structure of the unaltered olivine is close to Fo_{90} in good agreement with the XPS study. The Raman peaks located at about 881.0 cm^{-1}, 918.5 cm^{-1} and 960.5 cm^{-1} are attributed to B2g (ν_3 mode type), B3g (ν_3 mode type) and Ag (ν_3 mode type) symmetry modes, respectively.

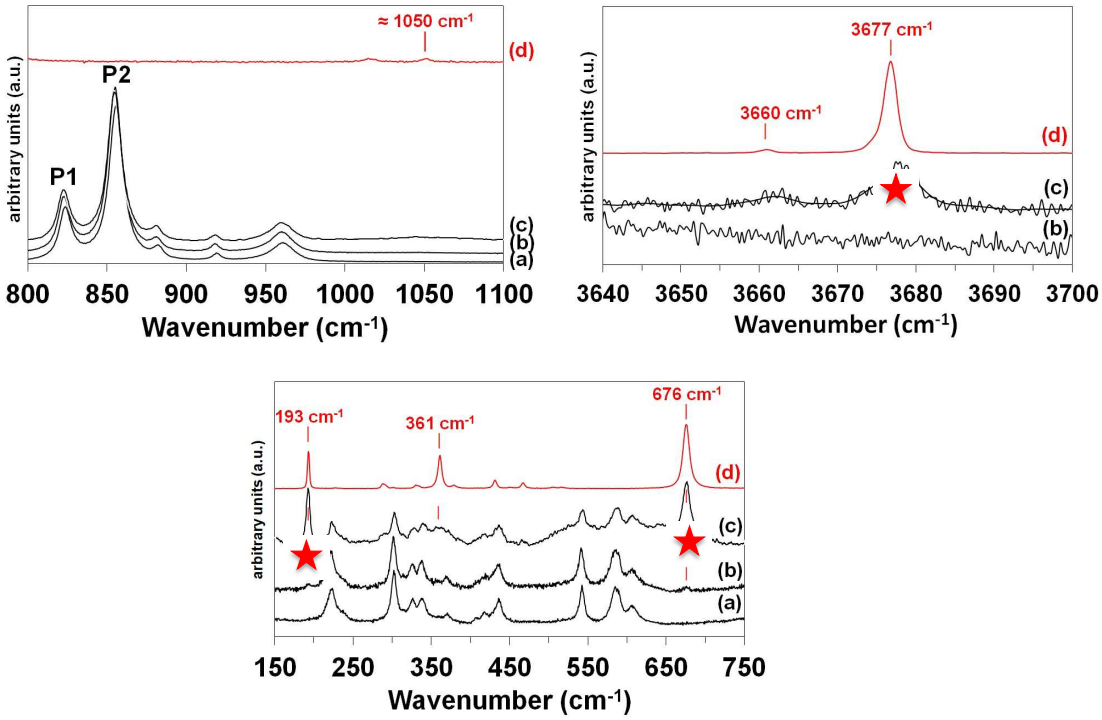

Figure 5: Raman spectra acquired from treated olivine samples V24 (a), V26 (b) and V27 (c), compared to a reference spectra of talc in red (d; Montagnac, 2000)

However, new peaks become visible for samples altered under water vapor pressure (indicated by stars, Fig. 5). In the spectral ranges of the vibrations of talc compound (150-1100 cm^{-1}) and the OH^- vibrational modes (3600–3700 cm^{-1}), three major Raman peaks can be identified at about 192.0 cm^{-1}, 675.3 cm^{-1} and 3678.1 cm^{-1}. Three minor Raman features were detected at 361.3 cm^{-1}, 1050 cm^{-1} and 3662.2 cm^{-1}. The peak at 192.0 cm^{-1} is assigned to the vibrational modes of an MO_6 octahedron ($Mg(O,OH)_6$, Loh, 1973), either distorted in the direction normal to the octahedral sheet (Blaha and Rosasco, 1978) or most likely from the lattice modes (Sontevska *et al.*, 2007, Jovanovski and Makreski, 2016, Kloprogge, 2017). The main Raman peak, located at 3678.1, is ascribed to □(OH) stretching modes (□(Mg_3OH)). In the spectral range of 3600 cm^{-1}-3700 cm^{-1}, only one Raman feature could be normally induced by hydroxyl groups (Blaha and Rosasco, 1978, Sharma *et al.*, 2010, Wang *et al.*, 2015, Kloprogge, 2017). According to these authors, the new peak (detected at 3662.0 cm^{-1}) is probably due to a slight structural distortion inducing non-equivalence in sites between the two OH groups. The second Raman peak could also be related to the presence of Fe^{2+} in the talc structure which affects the □(OH) vibrational modes; in this way, the Mg^{2+} cations are substituted by Fe^{2+} cations in the talc structure.

The status of Fe was investigated in more detail by X-ray Photo electron Spectroscopy. The limited depth of analysis of this spectroscopy allows us to better investigate the thin talc coating. Figure 6 reports the XPS Fe2p spectra of unaltered and altered olivine. For both the unaltered olivine and the sample altered under dry conditions, the presence of a satellite peak around 715-716 eV is mainly indicative of $Fe^{(II)}$ (Lin *et al.*, 1997, Yamashita and Hayes, 2008, Wilson and Langell, 2014). The same peak is observed for samples altered under vapor pressure, showing that, whatever the alteration conditions, we are unable to observe iron oxidation.

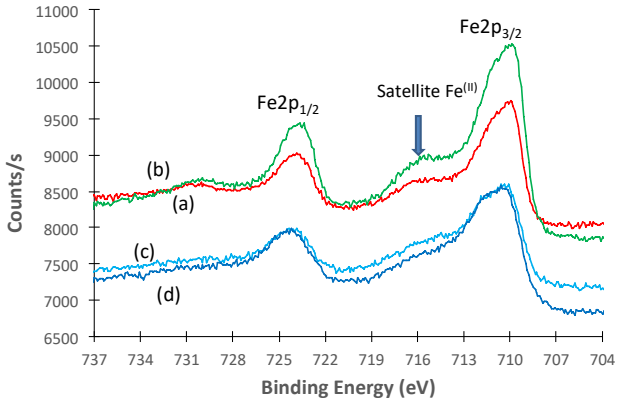

Figure 6: XPS Fe2p photoelectron spectra of unaltered (a) and altered San Carlos olivine samples under dry conditions (b-V24) and under vapor pressure (c-V26 and d-V27).

Evidence for the presence of talc is also provided by the OH- bonds visible by XPS on the O and Mg peaks reported in Figure 7.

On the unaltered olivine and the sample altered under dry conditions, the binding energy of Si2p at 101.8±0.1 eV and Mg1s at 1304.2 ± 0.1 eV is assigned to the Si-O-Mg chemical environment. For samples altered in water vapor (V26 and V27), the binding energy of Si2p at 103.1±0.1 eV corresponds to a $Si-(O)_4$ environment, while the signal of Mg1s at 1304.8±0.1 eV is characteristic of (HO)-Mg bonds. The high resolution spectrum of O1s confirms the presence of hydroxyl groups with the shift of the binding energy to 532.2 ±0.1 eV (Knipe *et al.*, 1995). The quantification of Si, Mg, Fe and O reported in Table 3 suggests a Si enrichment consistent with the formation of talc at the surface.

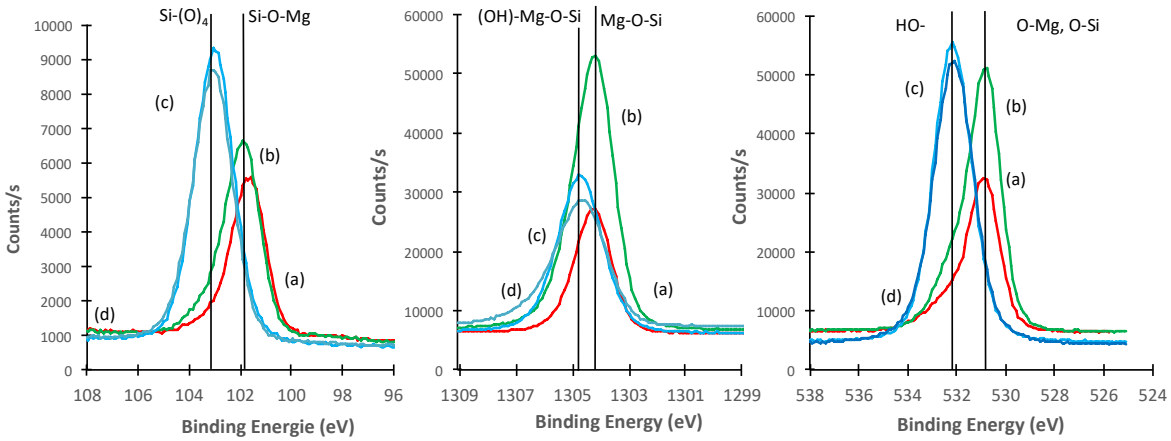

Figure 7: XPS of Si2p, Mg1s and O1s photoelectron spectra of unaltered (a) and altered San Carlos olivine samples under dry conditions (V24: b) and under water vapor pressure (V26: c), V27: d).

	Si		Mg		Fe		O	
	Si2p (eV)	Atom. %	Mg1s (eV)	Atom. %(Mg2s)*	Fe2p$_{3/2}$ (eV)	Atom. %	O1s (eV)	Atom. %
unaltered Ol.	101.7	16.8	1304.3	26.1	710.2	1.7	530.9	55.4
V24	101.8	16.4	1304.1	24.6	710.2	2.1	530.8	56.8
V26	103.0	23.7	1304.7	15.2	710.7	0.9	532.2	60.2
V27	103.2	23.5	1304.8	13.9	710.7	1.4	532.2	61.3

Table 3: XPS quantification of main elements present in unaltered and altered olivine samples. (*) For Mg, we use the Mg2s peak (not shown in Fig. 7) for a better quantification.

3.5 - Olivine in the picritic basalt:

The Fe-forsterite included in a basaltic rock, i.e. the picritic sample from Réunion Island, shows a different behavior. In addition to talc, we sometimes observed an iron-rich coating at the surface of the olivine grains. This coating is not systematically observed and the Raman spectroscopy of appropriate samples reveals the features of hematite. Figure 8 shows the spectra acquired in the low frequency region for the basalt samples V25 and V27, which were altered under dry and wet conditions, respectively. In comparison with other results (Wang *et al.*, 2015), hematite bands are clearly detected at about 224 cm^{-1} (with a weak shoulder at 245 cm^{-1}) as well as at 292 cm^{-1}, 406 cm^{-1} and 608 cm^{-1}. No (OH) vibrational modes characteristic of $FeO_{1+x}(OH)_{1-2x}$ compounds could be observed.

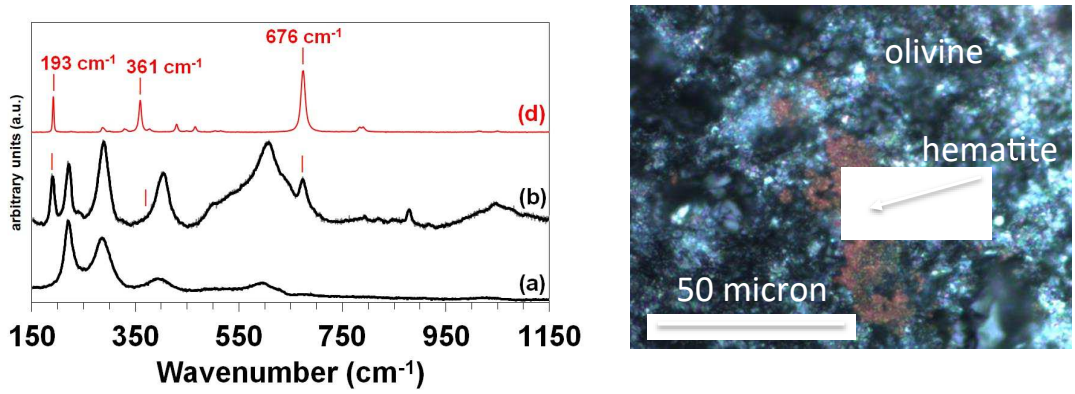

Figure 8: Raman spectra acquired for treated olivine samples in dry gas (V25, a) and in wet gas (V27, b), compared to the talc reference (d), and an example of the morphology of the corresponding surface (dry gas) observed with an optical microscope coupled to the Raman device.

Beside olivine, pyroxene (augite) also shows the presence of talc at its surface when altered under wet conditions, but only under the higher water vapor pressure (V27). Figure 9 shows the spectra of an augite-plagioclase mixture (left), the two phases being inevitably mixed together given the small size of the pyroxene crystals), with (OH) vibrational modes characteristic of the talc compound (right) at about 3662 cm^{-1} and 3676 cm^{-1}.

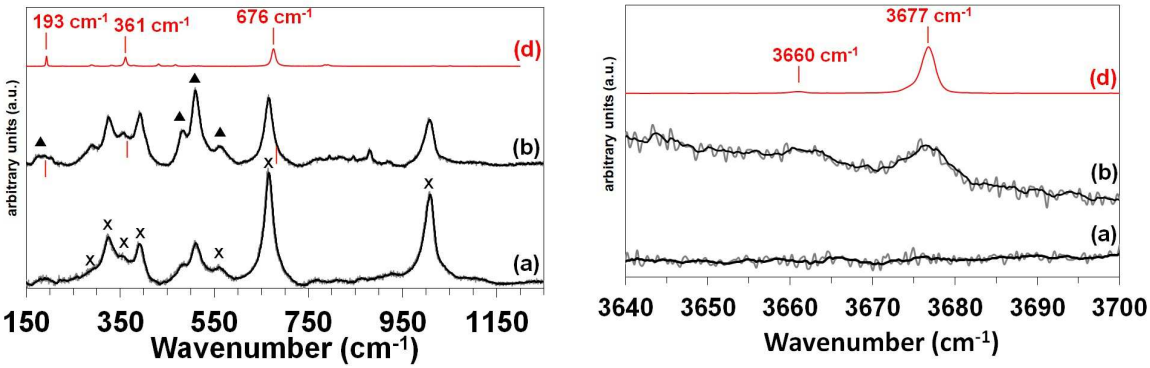

Figure 9: Raman spectra collected in the wavenumber ranges of 150-1200 cm^{-1} and 3640-3700 cm^{-1}, on sample V25 altered under dry conditions (a) and sample V27 altered under wet conditions (b). The spectra are compared to the talc reference (d). On the left, triangles and crosses indicate the Raman active vibrational modes of plagioclase and pyroxene, respectively.

4- Discussion and consequences for mechanisms occurring on geologic time scale

The experiments presented here are not designed to provide accurate rate constants for kinetic databases and numerical predictions. However, the mechanisms established in this study

allow us to assess how long glass and olivine will remain observable by remote sensing methods, according to geologic scenarios.

4.1 - Durability of glasses

The threshold water pressure required for glass alteration may constrain a geologic scenario for Venus surface alteration. Considering volcanic activity in the recent past or near future, and assuming the degassing of water-rich volatiles during this event, we can postulate that the maximum vapor pressure at the surface is limited by the atmospheric pressure. If pH_2O reaches 90 bar (fH_2O = 8.13 MPa) at low elevation on the plains, then any vitreous material of rhyolitic composition (low threshold water pressure) will undergo devitrification. For basaltic glasses requiring higher threshold water pressure for the recrystallization process, and provided that our short-term observations can be extrapolated on a geological time scale, the alteration will probably not be significant. This scenario may be generalized to any volcanic context and predicts that vitreous rhyolite (obsidian) should be rarer than vitreous basalt, which is generally the case at least on Earth.

In the Venus highlands, temperatures and pressures are lower than on the plains and approach hydrothermal conditions occurring on Earth. However, the T,P values never approach conditions for liquid water, so we can exclude the possibility of an aqueous Earth-like alteration at the present-day on Venus. Given a temperature of 300°C at 6 km elevation for the highlands and a corresponding pressure of 15 bar (much below the 85 bar required for liquid water), the water fugacity associated with a hydrous volcanic scenario will remain low, and consequently, both obsidian and basaltic dust or pebbles will remain vitreous as observed in our 300°C run. If alteration phases are found by future exploration missions in the highlands, or on the plains in a basaltic context, our experiments imply that these secondary phases are more likely to be relics of a past history when the greenhouse effect was weaker than today and associated with radically different T-P relationships. Combined with dating results, this could help to constrain the climate history.

It is also questionable if chemical modification of the glass sub-subsurface, the dominant process for basalt glass, would improve the chemical durability of the material. Since this modification is spontaneous, we can assume that it decreases the free energy of the system bringing it to an intermediate state between the pristine glass and the recrystallized glass under high water pressure. Figure 10 illustrates the hypothesis by which the chemically modified glass formed spontaneously under low water fugacity is more stable than the pristine glass.

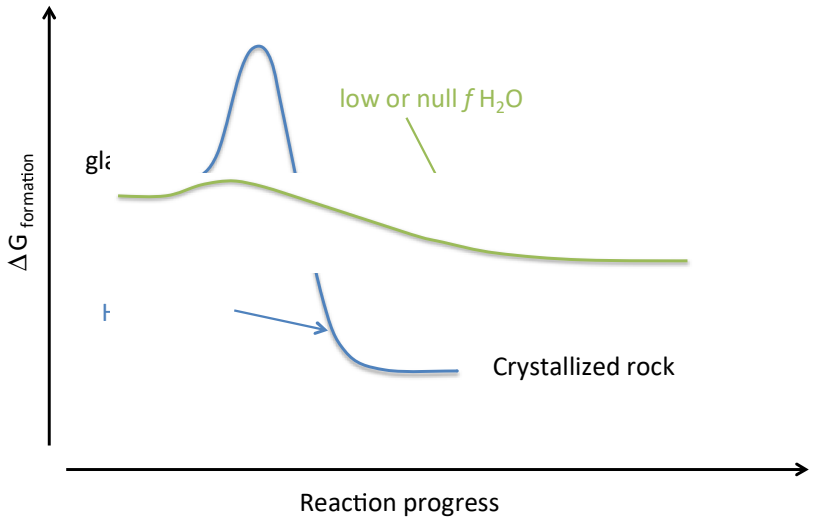

Figure 10: Assumption of the thermodynamic stability of glass alteration products: the crystallized assemblage at high water pressure is the more stable state of the system, while elemental migration below the surface occurring at low water pressure leads to an intermediate state with a higher durability than the pristine glass.

The propensity of a glass to evolve spontaneously by chemical migration near an interface is not specific to the present study. In an unpublished experimental study reported here, we heated a thin slab of the same tholeiitic glass at 1100°C for 20 hours under an Ar-10%H_2 gas flux at room pressure (measured pO_2= 5.10^{-23} bar). At this temperature, it is likely that water is not required to surpass the energy barrier shown in Fig. 10; the glass spontaneously recrystallized into the stable phases olivine, pyroxene and plagioclase. In fact, we observed an accumulation of plagioclase (Figure 11) reflecting elemental migration near the surface.

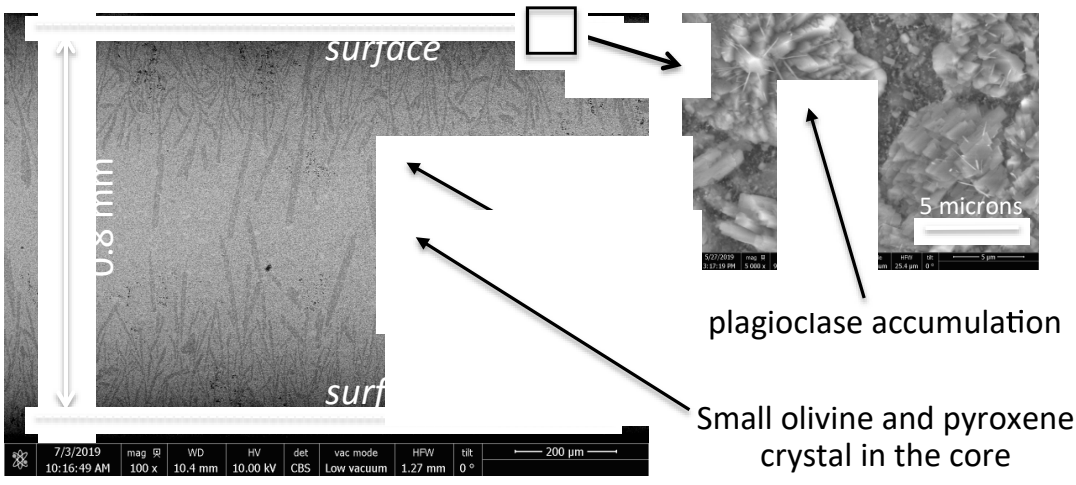

Figure 11: Chemical and mineralogical zoning occurring during heating of a polished section of tholeiitic glass at 1100°C for 20 hours under reducing conditions. The polished thin-section (left) shows an accumulation of Na-plagioclases near the surface, as identified by EDS analyses and observation of the surface (right).

4.2 - Durability of olivine

4.2.1 – reaction in dry gas

The only reaction observed under dry conditions is the development of an iron oxide coating on the olivine surface. However, the progress of this reaction is different according to whether it is reacted alone or within a rock. With the San Carlos sample, we failed to reproduce the observations of Berger et al. (2019). It is noteworthy that the redox conditions used in the present study, close to the expected values for the modern Venus surface (Zolotov, 2018; Semprich *et al.*, 2020), are not lower than the conditions applied by Berger *et al.* (2019) where iron oxide coatings were observed. A comparative illustration of redox conditions in different studies is reported in Figure 12. This supports the assumption that the formation of a Fe-coating, when observed, is not the consequence of fO_2 variations but is more likely due to another process.

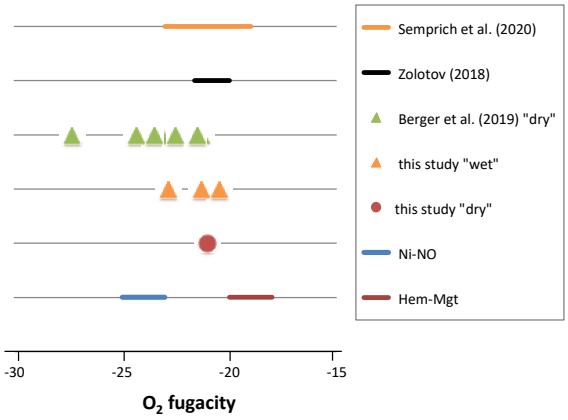

Figure 12: Comparison of the experimental redox conditions with the expected values for the modern Venus surface and the Ni-NiO and Hematite-Magnetite buffers.

A thick coating is absent at the surface of large isolated crystals of olivine, even though such a coating would be visible by SEM and optical microscopy. This suggests that, when observed, the iron coating is not produced at the expense of olivine itself but rather by adjacent minerals such as magnetite. The reactor itself, which is made of a Ni-based alloy,

cannot be a source of iron due to the surface passivation by Ni-oxides and the low mobility of Fe in the gas phase. However, several recent experimental studies have demonstrated that oxidation of Fe-bearing olivine and pyroxene at high temperature gives rise to iron oxides at the surface, owing to the diffusion of iron from the silicate lattice. Nevertheless, it should be noted that these studies were performed at higher temperature and, mostly, at higher O_2 fugacity: 600°C in air in the case of Cutler *et al.*, 2020; 600-900°C in air for Knafelec *et al.*, 2019; with shock samples up to 59 GPa for Mc Canta *et al.*, 2020. The lower O_2 fugacity, shorter run times and less extreme conditions of the present study do not allow surface oxidation since this would be controlled by the slow solid-state diffusion of iron through the underlying olivine.

Our own observations are fairly consistent with what is known about diffusion kinetics at mineral surfaces. Balluffi *et al.* (2005) discussed different diffusion processes and reported diffusivity values as a function of temperature, more exactly the ratio of diffusivity to melting temperature. In Figure 13, we extrapolate Balluffi *et al.'s* (2005) reported diffusivity data along a free surface to our experimental temperatures, obtaining value of the order of 10^{-17} m^2/s. This value is equivalent to the diffusivity in a bulk crystal at 1100°C, a temperature at which it is accepted that elemental migration is not significant after only one week. The formation of the observed iron coating after one week at 475°C is better explained by surface diffusion from an adjacent iron-rich mineral (magnetite?).

a. Notation for short-circuit diffusivities

D^D (unidissoc)	Diffusivity along an undissociated core (i.e. a cylinder, or a "pipe" of diameter, δ)
D^D (dissoc)	Diffusivity along a dissociated dislocation core (i.e. a cylinder, or a "pipe" of diameter, δ)
D^B	Diffusivity along a grain boundary (i.e. a slab of thickness, δ)
D^S	Diffusivity along a free surface (i.e. a slab of thickness, δ)
D^{XL}	Diffusivity in a bulk crystal free of line or planar imperfection
D^L	Diffusivity in a liquid

b. Diffusivities vs reduced temperature

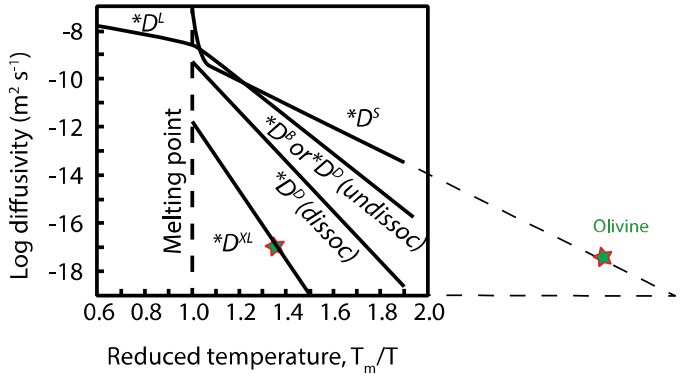

Figure 13: Extrapolation of the diffusivity along a free surface from data of Ballufi et al. (2005) to our experimental conditions. The red star corresponds to 10^{-17} m^2/s, a value close to the diffusivity in a bulk crystal at 1100°C

This assumption takes also into account the absence of enstatite, expected to be associated with iron oxide but which is not observed by Berger e*t al.* (2019), which should form according to the reaction Fe-forsterite + ½ O_2 = hematite + enstatite, or fayalite = FeO + enstatite (Zolotov *et al.,* 2017). This also supplements the discussion of Filiberto *et al.* (2020) on the detectability of olivine in Venus lava flows. The spontaneous coating of olivine by iron oxide is an argument for the non-detection of olivine on the surface of Venus by remote sensing, except for unaltered fresh material. It can be used to estimate the age of lava flows when olivine is still visible. However, an accurate estimation of olivine lifetime based on remote sensing requires an accurate knowledge of the implied processes. Surface diffusion from grain to grain is a fast process which should be considered when easily accessible sources of iron (oxides, nanophases, etc.) are present in the basalt.

4.2.2 – reaction in wet gas

One of the highlights of this study is the relative stability of olivine exposed to the temperatures and high water-pressures occurring on Venus. We only observed a thin Fe,Mg-talc layer at the surface and only a trace of hematite was detected by Raman spectroscopy. The absence of a significant iron oxide coating on olivine crystals within the picritic basalt may suggest that the surface diffusion of iron is precluded or hindered by the interaction of H_2O molecules with the mineral surfaces leading to the formation of OH-bearing groups (or even talc in the case of olivine).

The apparent stability of olivine under supercritical conditions has already been observed by other experimenters (Martin and Fyfe, 1970, Wegner and Ernst, 1983, Allen and Seyfried, 2003, McCollom *et al.*, 2016). This stability contrasts with the faster serpentinization of olivine at lower temperatures resulting from the hydrolysis of olivine by the protons in the solution, followed by the precipitation of 1:1 silicate from the serpentine mineral and magnetite, +/- brucite (Moody, 1976). The reaction kinetics is not only dependent on pH and temperature but also on water fugacity (Lamadrid *et al*., 2017). In the present study conducted under supercritical conditions, we do not observe the oxidation of Fe^{++} by water and incorporation of Fe and Mg in separate phases. Fe-bearing talc seems rather to form

directly from olivine by a local atomic rearrangement. However, this topotactic-like reaction is not isochemical. H_2O and silica are either supplied by an external source corresponding to the gas phase, or, alternatively, a fraction of Mg is lost in the gas. Such exchanges with the gas phase are conceivable but, contrary to the context of an aqueous solution, the gas phase is not a significant solvent able to sustain dissolution of cations or give rise quantitatively to the growth of a newly formed silicates (by contrast with sulfide/sulfate, carbonate, chloride). Rather than a dissolution-precipitation process, a topotactic reaction seems more likely in this case.

The 2:1 structure of talc, as revealed by XRD and laser spectroscopy, reflects the non-isochemical feature of the reaction. Talc contains more silica than forsterite, as illustrated by the following chemical reaction:

$$(Mg_{0.9}Fe_{0.1})_2SiO_4 + H_2O + 2.5\ SiO_2 = Mg_{2.7}\,Fe_{0.3}Si_4O_{10}(OH)_2$$

(San Carlos olivine) *(talc)*

In a strictly closed system, the olivine + H_2O reaction predicted by thermodynamics produces a 1:1 Mg-phyllosilicate from the serpentine mineral (antigorite) and magnetite is formed as a sink for iron.

The formation of talc, instead of antigorite, supposes an external source of silica. In the particular case of our experiments, the source of silica may be either the other samples present in the Pt crucible, such as the glass slabs for example, or a more likely contamination of the gas by the reactor itself. Berger *et al.*, 2019 reported a blank level higher than 200 ppb for SiO_2 in the gas in the same reactor and at the same P-T conditions. The transfer of silica mediated by the gas phase is particularly efficient under high water pressure. Plyasunov (2011) calculated the solubility of H_4SiO_4 under aqueous supercritical conditions of the order of 10^{-2}% mol for a water density of 0.17 (≈#V27) at 500°C. By comparison, this value corresponds to the solubility of amorphous silica in water at 100°C. Any spatial variation of chemical potential of the silica (from glass to olivine surface, for example) may easily generate a mass transfer.

The relative stability of olivine during one week at 475°C and 100 bar water pressure also raises the question of whether thermodynamics or kinetics control the progress of the reaction,. When approaching 500°C, the thermodynamic force driving olivine serpentinization decreases (the bell-shaped dependency shown in Brunet, 2019) and is close to chemical equilibrium. However, thermodynamic considerations prevail in a rock-dominated closed system where the influence of fluid composition is negligible, in particular for the redox

status of iron. In an open system, the stability of serpentine minerals (up to 600°C, Bromiley and Pawley, 2003) may allow the reaction in the supercritical region, provided the fluid remains undersaturated with respect to olivine. Because of the excess of the gas phase compared to the small surface-area of olivine, our experimental system may be rather considered as an open system with a steady state fluid composition. The oxidation potential (hematite coating) and the source of silica (talc instead of antigorite) are assumed to drive the transformation of olivine, but this reaction is only observed to a very limited extent. We could consider that the source of silica (by contamination from the reactor or transfer from neighboring samples) is exhausted with time, thus stopping the reaction, but this assumption is unlikely. This is also the case for the surface of Venus, where a source of silica can easily be envisaged, or for volcanic degassing where water-bearing gas has a significant silica content.

It is difficult to give a definitive conclusion here in the absence of a dedicated kinetic study exploring other factors like run duration or the progress (or not) of olivine alteration after renewal of the gas phase. Nevertheless, given the close association between primary olivine and secondary talc, we are rather in favor of a passivation effect by which talc protects the underlying olivine from hydration and oxidation as illustrated in Figure 14.

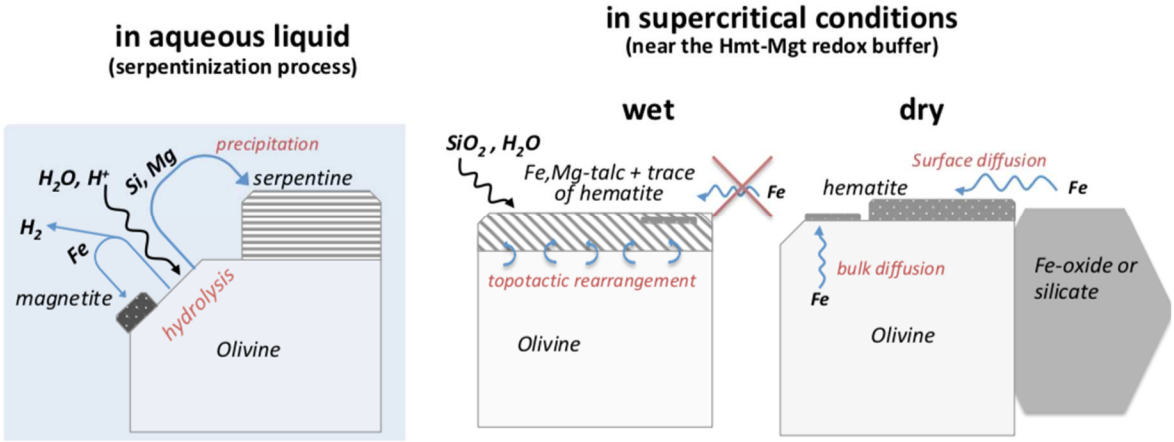

Figure 14: Scheme depicting different alteration mechanisms of olivine: dissolution-precipitation in a liquid aqueous fluid (left), a local rearrangement including water and silica from the supercritical phase (middle) and Fe-oxides coating under dry hot gas (right)

Previous authors have envisaged a passivation effect involving secondary iron oxy-hydroxides at the olivine surface (Sissmann *et al.*, 2013; Saldi *et al.*, 2013; Saldi *et al.* (2015). This effect could also contribute to the decrease in serpentinization rate at high temperature

631 reported by other experimenters (Martin and Fyfe, 1970, Wegner and Fyfe, 1983). On that
632 basis, we can compare our observations with previously published kinetic studies.
633 Considering a talc layer thickness of few microns after one week of reaction, we obtain an
634 average alteration rate of the order of 10^{-7} mol.m^{-2}.s^{-1} at 470°C, a value that is not radically
635 different from the serpentinization rates at lower temperatures reported in Lamadrid *et al.*
636 (2017). Our assumption implies that serpentinization of ultramafic rocks at high temperature
637 may not be as intense as might be considered in deep Earth crust or at the Early Venus surface.
638 This decrease in serpentinization rate may then be attributed to a change in the reaction
639 mechanism under supercritical conditions.
640 We find no evidence for the formation of Mg-carbonate either, while numerous
641 published studies (see Introduction) report that Ca or Mg carbonates are readily formed in wet
642 CO_2 gas, with the carbonation reactions being promoted by the sorption of a water film at the
643 mineral surfaces. The absence of carbonation in our experiments may indicate that such a
644 water film does not form at around 500°C (or does not have the same properties as at lower
645 temperatures). Alternatively, the competition with other by-products, namely sulfates, is not
646 in favor of carbonates.
647
648 4.3 – Importance of Water Diffusion.

649 Finally, for both glass and olivine under low-density supercritical conditions, the controlling
650 factor of reaction rate is probably not the gas interface and the organization of the first
651 molecular layers in the fluid (the Helmholtz layer as described in Crundwell, 2014). We
652 consider that it is due rather to the rearrangement of solid phases in the first atomic layer
653 beneath the surface and at greater depth. In this case, the characteristic distance of diffusion (a
654 parameter derived from Fick's law) characterizes the extent of diffusion of components, in
655 particular water molecules, through the crystals and volcanic glasses at a given temperature
656 and time; this characteristic distance may be compared to our observations in terms of
657 thickness of the altered layer. For silicate glasses, Okumura and Nakashima (2006) compiled
658 numerous previous studies and reported water diffusion coefficients from their own
659 experiments in the 400-675°C range for glasses of different composition. It appears that the
660 variation of diffusivity with glass composition is complex, due to the fact that all chemical
661 components, including water itself, have different roles in silicate structures. Applied to our
662 time-temperature conditions, and assuming 0.7% water in the glass as considered by Okumura
663 and Nakashima (2006), the characteristic distance ($\sqrt{D_i t}$) is of the order of 23 µm for the

basalt glass and 123 µm for the rhyolite glass. These calculated values are smaller but remain in the same order of magnitude as those reported in Fig.2. Although these values clearly depend on the initial water content in the glass, the ratio between the characteristic distances (i.e. the thickness of the altered layer in a basalt glass compared with a rhyolitic glass) is close to our observations (which also depends on fH_2O in the gas). For olivine, we obtain a characteristic distance for one week of 0.27 micron whatever the crystallographic axis. This distance is calculated using the diffusion coefficient of water in forsterite reported in the literature (Demouchy and Mackwell, 2003), extrapolated to 475°C and assuming an average activation energy of 210 $kJ.mol^{-1}$ proposed by these authors. This very low value is consistent with the absence of a significant alteration layer at the olivine surface in our experiments.

These considerations support our hypothesis that (the lack of) diffusion of water inside silicate minerals is crucial for their chemical resistance to supercritical fluids. For glass, which is "permeable" to water, the diffusion of H_2O molecules promotes the diffusion of other elements like Ca and Na leading to a modified (perhaps more resistant) layer. For olivine, the diffusion is negligible near 500°C and a (passive?) layer of talc as shown in Figure 13 leads to a molecular rearrangement of the surface incorporating both H_2O and SiO_2 from the gas. In both olivine and glass, the alteration is less pronounced under supercritical conditions at high temperatures than under hydrothermal conditions at lower temperatures.

5- Conclusion

The complementary nature of the surface analyses reported in this study allow us to better unravel the reactions controlling the alteration rate of glass and olivine under H_2O-CO_2 based supercritical conditions, such those prevailing on ancient Venus and more generally in volcanic environments.

By incorporating results from previous published studies, it appears that vitreous materials are sensitive to a water pressure threshold depending on glass composition. Below this threshold, the reaction is limited to elemental mobility in the glass (alkali enrichment, calcium loss) leading to a (?more stable) surface layer of tens to hundreds of microns. Above this threshold water pressure, roughly 50 bar H_2O for an obsidian but >250 bar H_2O for a tholeiitic glass, water promotes the depolymerization of glass and the crystallization of stable minerals. This crystalline rim is less protective than the chemically modified layer and propagates more quickly than the diffusion in the glass, at least for obsidian. According to this scheme, the bulk aqueous alteration of Venusian basalt is unlikely at high temperatures and

requires a pH_2O-temperature relationship radically different from the present-day situation (plains or highlands).

Olivine reacts differently whether it is isolated or included in a basaltic rock. Iron coatings, identified here as hematite, are only formed in the latter case, suggesting that, for the timescale and redox conditions of our experiments, these coatings are not fed by olivine itself but rather by surface diffusion from neighboring Fe-rich phases. Nevertheless, this supports previous experimental studies and orbital observations concerning the short-term visibility of "unaltered" olivine in Venus lava flows. Indeed, the isolated olivine crystals tested in our study help to improve our understanding of the surface processes, but do not correspond to a natural situation. On the surface of Venus, olivine has so far been detected only as being included in basalt and is thus closely connected to other Fe-bearing minerals promoting the spontaneous formation of iron coatings.

Under high water vapor pressure, Fe-bearing talc likely crystallizes from a topotactic-like reaction. Under our experimental conditions, the formation of talc, a Si-rich phyllosilicate, implies a source of silica external to olivine itself, perhaps the accompanying glass samples. In a natural environment dominated by a wet gas phase, such as associated with volcanic degassing or an ancient climate in the case of Venus, sources of silica are expected in a basaltic context; our experimental results predict the formation of talc provided there is a significant water fugacity. The structure of this micrometric talc layer may represent a protective layer giving the illusion that olivine and H_2O can coexist stably owing to a reversible chemical equilibrium. Ultimately, olivine is a sink for both silica and iron coming from the neighboring rock-forming minerals and this local elemental mobility should be kept in mind when modeling Venus surface reactions.

Acknowledgements

This research did not receive any specific grant from funding agencies in the public, commercial or not-for-profit sectors. The authors would like to thank the 'Laboratoire de Géologie de Lyon', France (INSU, CNRS) for access to the Handbook of Raman spectra for geology (http://www.geologie-lyon.fr/Raman/). This database is currently being rebuilt under a new name: REAP (Raman Experiments for Astrobiology and Planetology), described on the same website.

The manuscript was greatly improved based on the comments and remarks made by Benjamin Tutolo (University of Calgary), Justin Filiberto (LPI, TX,US) and an anonymous reviewer.

731 The English style and grammar was post-edited by Dr M.S.N. Carpenter.

732

733

References

Allen D.E., and Seyfried W.E. (2003) Compositional controls on vent fluids from ultramafic-hosted hydrothermal systems at mid-ocean ridges: An experimental study at 400°C, 500 bars, *Geochim. Cosmochim. Acta* **67**, 1531–1542

Martin B., and Fyfe W.S. (1970) Some experimental and theoretical observations on the kinetics of hydration reactions with particular reference to serpentinization, *Chem. Geol.* **6**, 185-195

Balluffi R.W., Allen S.M. and Carter W.C. (2005) Kinetics of materials. Wiley-Interscience, Hoboken, N.J. editors, John Wiley & Sons. ISBN: 9780471749318

Bakker R.J. (2009) Package FLUIDS. Part 3: correlations between equations of state, thermodynamics and fluid inclusions. *Geofluids* **9**, 63–74.

Berger G., Cathala A., Fabre S., Borisova A. Pages A. Aiguy T. and Esvan J. (2019) Experimental investigation of volcanic rocks-atmosphere interaction under Venusian surface conditions. *Icarus* **329**, 8-23

Breitenfeld L.B., Dyar M.D., Carey C.J., Tague T.J. Jr, Wang P., Mullen T. and Parente M. (2018) Predicting olivine composition using Raman spectroscopy through band shift and multivariate analyses. *Am. Mineral.* **103**, 1827-1836

Bromiley G.D. and Pawley A.R. (2003) The stability of antigorite in the systems MgO-SiO_2-H_2O (MSH) and MgO-Al_2O_3-SiO_2-H_2O (MASH): The effects of Al^{3+} substitution on high-pressure stability. *Am. Mineral.* **88**, 99-108

Brunet F. (2019) Hydrothermal Production of H_2 and Magnetite From Steel Slags: A Geo-Inspired Approach Based on Olivine Serpentinization. *Front. Earth Sci.* **7**, 17

Cutler K.S., Filiberto J., Treiman A.H., Trang D. (2020) Experimental Investigation of Oxidation of Pyroxene and Basalt: Implications for spectroscopic analyses of the surface of Venus and the ages of lava flows. *The Planet. Sci. Journal* **1**, 21

Daval D., Martinez I., Corvisier J., Findling N., Goffé B. and Guyot F. (2009) Carbonation of Ca-bearing silicates, the case of wollastonite: Experimental investigations and kinetic modeling *Chem. Geol.* **265**, 63–78

Delmelle P., Wadsworth F.B., Maters E.C. and Ayris P.M. (2018) High temperature reactions between gases and ash particles in volcanic eruption plumes. *Rev. Mineral. Geochem.* **84**, 295–308

Demouchy S. and Mackwell S. (2003) Water diffusion in synthetic iron-free forsterite. *Phys. Chem. Miner.* **30**, 486-494

Fegley Jr. B., Zolotov M.Y. and Lodders K. (1997). The oxidation state of the lower atmosphere and surface of Venus. Icarus 125, 416–439

Filiberto J., Trang D., Treiman A.H. and Gilmore M.S. (2020) Present-day volcanism on Venus as evidenced from weathering rates of olivine. *Sci. Adv.* **6**, eaax7445

Ishibashi H., Arakawa M., Ohi S., Yamamoto J., Miyake A. and Kagi H. (2008) Relationship between Ramen spectral pattern and crystallographic orientation of a rock-forming mineral: A case study of $Fo_{89}Fa_{11}$ olivine. *J. Raman Spectrosc.* **39**, 1653-1659

Jovanovski G. and Makreski P. (2016) Minerals from Macedonia. XXX. Complementary use of vibrational spectroscopy and X-ray powder diffraction for spectra-structural study of some cyclo-, phyllo- and tectosilicate minerals. A review. *Maced. J. Chem. Chem. Eng.*

35, 125–155

King P.L., Wheeler V.M., Renggli C.J., Palm A.B., Wilson S.A., Harrison A.L., Morgan B., Nekvasil H., Troitzsch U., Mernagh T., Yue L., Bayon A., DiFrancesco N.J., Balie R., Kreider P. and Lipinski W. (2018) Gas-solid reactions: theory, experiments and case studies relevant to earth and planetary processes. *Rev. Miner. Geochem.* **84**, 1–56

Kloprogge J.T. (2017) Chapitre 6 - Raman spectroscopy of Clay Minerals. *Dev. Clay Sci.* **8**, 150-199

Knafelc J., Filiberto J., Ferré E.C., Conder J.A., Costello L., Crandall J.R., Dyar M.D., Friedman S.A., Hummer D.R., Schwenzer S.P. (2019) Effect of oxidation on the mineralogy and magnetic properties of olivine. *Am. Mineral.* 1**04**, 694-702

Knipe S.W., Mycroft J.R., Pratt A.R., Nesbitt H.W. and Bancroft G.M. (1995) X-ray photoelectron spectroscopic study of water adsorption on iron sulphide minerals. *Geochim. Cosmochim. Acta* **59**, 1079-1090

Kuebler K.E., Jolliff B.L., Wang A. and Haskin L.A. (2006) Extracting olivine (Fo-Fa) compositions from Raman spectral peak positions. *Geochim. Gosmochim. Acta* **70**, 6201-6222

Lamadrid H.M., Rimstidt J.D., Schwarzenbach E.M., Klein F., Ulrich U., Dolocan A. and Bodnar R.J. (2017) Effect of water activity on rates of serpentinization of olivine. *Nat. Commun.* **8,** 16107

Lin T.-C., Seshadri G.J. and Kelber A. (1997), A consistent method for quantitative XPS peak analysis of thin oxide films on clean polycrystalline iron surface, *Appl. Surf. Sci.* **119**, 83-92

Loh E. (1973) Optical vibrations in sheet silicates. *J. Phys. C: Solid State Phys.* **6**, 1091-1103

Martin B. and Fyfe W.S. (1970) Some experimental and theoretical observations on the kinetics of hydration reactions with particular reference to serpentinization. *Chem. Geol.* **6**, 185-202

McCanta M.C., Dyar M.D. (2020) Effects of oxidation on pyroxene visible-near infrared and mid-infrared spectra. *Icarus* **352**, 113978

Miller Q. R.S, Schaef H. T., Kaszuba J. P., Gadikota G., McGrail B. P. and K. M. Rosso (2019) Quantitative review of olivine carbonation kinetics: Reactivity trends, mechanistic insights, and research frontiers. *Environ. Sci. Technol. Lett.* **6**, 431–442

Moody J.B. (1976) Serpentinization: A review. *Lithos* **29**, 125-138

Okumura S. and Nakashima S. (2006). Water diffusion in basaltic to dacitic glasses. *Chem. Geol.* **227**, 70-82

Palm A.B., King, P.L., Renggli, C.J., Hervig R.L., Dalby K.N., Herring, A., Mernagh T.P., Eggins S.M., Troitzsch U., Beeching L., Kinley L. and Guagliardo P. (2018) Unravelling the consequences of SO_2-basalt reactions for geochemical fractionation and mineral formation. *Rev. Mineral. Geochem*. **84**, 257–283

Parques-Ledent M.T. and Tarte P. (1973) Vibrational studies of olivine-type compound I. The IR and Raman spectra of the isotopic species of Mg_2SiO_4. *Spectrochim. Acta, Part A* **29**, 1007-1016

819 Piriou B. and McMillan P. (1983) The high-frequency vibrational spectra of vitreous and
820 crystalline orthosilicates. *Am. Mineral.* **68**, 426-443

821 Plyasunov A.V. (2011) Thermodynamic properties of H_4SiO_4 in the ideal gas state as
822 evaluated from experimental data. *Geochim. Cosmochim. Acta* **75**, 3853-3865

823 Renggli C.J. and King P.L. (2018) SO_2 gas reactions with silicate glasses. *Rev. Mineral.*
824 *Geochem.* **84**, 229–255

825 Regnault O., Lagneau V. and Schneider, H. (2009) Experimental measurement of portlandite
826 carbonation kinetics with supercritical CO_2. *Chem. Geol.* **265**, 113–121

827 Saldi G.D., Daval D., Morvan G. and Knauss K.G. (2013) The role of Fe and redox
828 conditions in olivine carbonation rates: an experimental study of the rate limiting reactions
829 at 90 and 150 °C in open and closed systems. *Geochim. Cosmochim. Acta* **118**, 157–183

830 Saldi G.D., Daval D., Guo H., Guyot F., Bernard S., Le Guillou C., Davis J.A. and Knauss,
831 K.G. (2015) Mineralogical evolution of Fe–Si-rich layers at the olivine-water interface
832 during carbonation reactions. *Am. Mineral.* **100**, 2655–2669

833 Savary V., Berger G., Dubois M., Lacharpagne J.C., Pages A., Thibeau S. and Lescanne L.
834 (2012) The Solubility of CO_2 + H_2S Mixtures in Water and 2 M NaCl at 120°C and
835 Pressures up to 35 MPa. *Inter. J. Greenhouse Gas Control* **10**, 123-133

836 Semprich J., Filiberto J., Treiman A.H. (2020) Venus: A phase equilibria approach to model
837 surface alteration as a function of rock composition, oxygen- and sulfur fugacities. *Icarus*
838 **346**, 113779

839 Sharma S.K., Misra A.K., Clegg S.M., Barefield J.E., Wiens R.C. and Acosta T. (2010) Time-
840 resolved remote Raman study of minerals under supercritical CO_2 and high temperatures
841 relevant to Venus exploration. *Phil. Trans. R. Soc.* **368**, 3167–3191

842 Sissmann O., Daval D., Brunet F., Guyot F., Verlaguet A., Pinquier Y., Findling N. and
843 Martinez I. (2013) The deleterious effect of secondary phases on olivine carbonation yield:
844 insight from time-resolved aqueous-fluid sampling and FIB-TEM characterization. *Chem.*
845 *Geol.* **357,** 186-202

846 Sontevska V., Jovanovski G., Makreski P. (2007) Minerals from Macedonia. Part XIX.
847 Vibrational spectroscopy as identificational tool for some sheet silicate minerals. *J. Mol.*
848 *Struct.* **834-836,** 318–327

849 Thompson C.J., Loring J.S., Rosso K.M., Wang Z. (2013) Comparative reactivity study of
850 forsterite and antigorite in wet supercritical CO_2 by in situ infrared spectroscopy. *Inter. J.*
851 *Greenhouse Gas Control* **18**, 246-255

852 Wang A., Freeman J.J. and Jolliff B.L. (2015) Understanding the Raman spectral features of
853 phyllosilicates. *J. Raman Spectrosc.* **46,** 829-845

854 Wegner W.W. and Ernst W.G. (1983) Experimentally determined hydration and dehydration
855 reaction rates in the system MgO-SiO_2-H_2O. *Amer. J. Sci.* **283**, 151-180

856 Wilson D. and Langell M.A. (2014) XPS analysis of oleylamine/oleic acid capped Fe_3O_4
857 nanoparticles as a function of temperature. *Appl. Surf. Sci.* **303**, 6-13

858 Yamashita T. and Hayes P. (2008) Analysis of XPS spectra of Fe^{2+} and Fe^{3+} ions in oxide
859 materials, *Appl. Surf. Sci.* **254**, 2441-2449

860 Zolotov M.Y. (2018) Gas-solid interactions on Venus and other solar system boides. *Rev.*
861 *Miner. Geochem.* **48**, 351-392

Table captions

Table 1: Experimental conditions for basalt glass and olivine reaction under Venus conditions. $X(H_2O)$ is the water molar ratio in the gas and d the density at the working temperature.

Table 2. Chemical composition of the starting samples. (*) described in Berger et al. (2019)

Table 3: XPS quantification of main elements in unaltered and altered olivine samples. (*) For Mg we used the Mg2s peak (not shown in Fig. 7) for a better quantification.

Figure captions

Figure 1: SEM observation in backscattering mode of the modified layer in a reacted tholeiitic glass sample altered under high vapor pressure (V27, polished section). Linescans of EDS point analyses in the modified layer are reported on the right.

Figure 2: Dependence of tholeiitic glass alteration thickness on water fugacity, compared with the recrystallized rim thickness of obsidian glass reported in Berger et al. (2019). The vertical dashed lines indicate the threshold values for the onset of alteration.

Figure 3: SEM observation in backscattering mode of the leached layer in an obsidian glass sample reacted in water vapor at 300°C (V28, polished section). The accumulation of elements is visible by the color contrast (elemental compositions measured by EDS).

Figure 4: SEM images of single San Carlos crystals reacted one week at 475°C under 247 bar (upper left) and 320 bar (upper right) H_2O-CO_2 pressure, with XRD pattern of the surface in grazing incidence.

Figure 5: Raman spectra acquired from treated olivine samples V24 (a), V26 (b) and V27 (c), compared to a reference spectra of talc in red (d; Montagnac, 2000).

Figure 6: XPS Fe2p photoelectron spectra of unaltered (a) and altered San Carlos olivine samples under dry conditions (b-V24) and under vapor pressure (c-V26 and d-V27).

Figure 7: XPS of Si2p, Mg1s and O1s photoelectron spectra of unaltered (a) and altered San Carlos olivine samples under dry conditions (V24: b) and under water vapor pressure (V26: c), V27: d).

Figure 8: Raman spectra acquired for treated olivine samples in dry gas (V25, a) and in wet gas (V27, b), compared to the talc reference (d), and an example of the morphology of the corresponding surface (dry gas) observed with an optical microscope coupled to the Raman device.

Figure 9: Raman spectra collected in the wavenumber ranges of 150-1200 cm^{-1} and 3640-3700 cm^{-1}, on sample V25 altered under dry conditions (a) and sample V27 altered under wet conditions (b). The spectra are compared to the talc reference (d). On the left, triangles and crosses indicate the Raman active vibrational modes of plagioclase and pyroxene, respectively.

Figure 10: Assumption of the thermodynamic stability of glass alteration products: the crystallized assemblage at high water pressure is the more stable state of the system, while elemental migration below the surface occurring at low water pressure leads to an intermediate state with a higher durability than the pristine glass.

Figure 11: Chemical and mineralogical zoning occurring during heating of a polished section of tholeiitic glass at 1100°C for 20 hours under reducing conditions. The polished thin-section (left) shows an accumulation of Na-plagioclases near the surface, as identified by EDS analyses and observation of the surface (right).

Figure 12: Comparison of the experimental redox conditions with the expected values for the modern Venus surface and the Ni-NiO and Hematite-Magnetite buffers.

Figure 13: Extrapolation of the diffusivity along a free surface from data of Ballufi et al. (2005) to our experimental conditions. The red star corresponds to 10-17 m2/s, a value close to the diffusivity in a bulk crystal at 1100°C.

Figure 14: Scheme depicting different alteration mechanisms of olivine: dissolution-precipitation in a liquid aqueous fluid (left), a local rearrangement including water and silica from the supercritical phase (middle) and Fe-oxides coating under dry hot gas (right).